Chapter 2

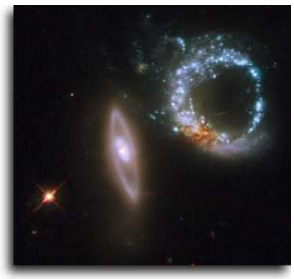

Simulated supernova survey strategies

2.1 Introduction

Given that past SN survey strategies have been biased towards higher-metallicity events (see Section 1.4), it is inherently interesting to search for SNe in specifically low-metallicity environments, or at least searching with a survey strategy that is not biased towards high metallicity regimes. In this chapter several strategies to search for low-metallicity CCSN events shall be considered and discussed.

By compiling catalogues of star-forming galaxies, the total rates of CCSNe hosted within the volumes searched by these survey strategies are estimated. These CCSN rates are given as a function of oxygen abundance. Monte Carlo simulations are then used to estimate the CCSN discovery efficiency for each strategy. With this combined information it is possible to predict the CCSN discovery rates for each survey strategy. Within any survey a SN will only be discovered if it is bright enough to be detected at the point of observation. The factors that influence the likelihood that a CCSN will be discovered include whether or not it is in solar conjunction, the type of CCSN concerned (IIP, IIL, Ibc or IIn) and its intrinsic brightness, the age of the CCSN when observed (affected by the cadence of the observations), the distance to the host galaxy, the extinction towards the CCSN and the limiting magnitude of the survey. The Monte Carlo simulations take account of these various survey parameters, giving them appropriate weights, and are used to generate a random sample of 100,000 CCSNe potentially observable within each survey strategy. From this sample it is possible to estimate the fraction of CCSNe that should be discovered with each strategy. Driven by the ambition of designing a survey strategy optimised to detect CCSNe in the nuclear regions of nearby starburst galaxies, Mattila and Meikle (2001) have developed Monte Carlo Simulations to search for supernovae in K-band images of NGC 5962. The structure of the Mattila and Meikle (2001) simulations is used purely as a model framework on which to build the Monte Carlo Simulations developed in this chapter. I have created these Monte Carlo Simulations to account for all the parameters specific to the various survey strategies considered here (cadence of observations, limiting-magnitudes, filters) and the CCSNe they are designed to discover (weighted distributions of distance, type, peak magnitudes, extinctions and the CCSN rates).

In Section 2.2 a description of the compilation of star-forming galaxy catalogues from the Sloan Digital Sky Survey Data Release 5 is given. Oxygen abundances, star-formation rates and CCSN rates are determined for these galaxies. A total of three survey strategies designed to search for CCSN hosted by low-metallicity galaxies are considered. For each strategy a Monte Carlo simulation is written and used in conjunction with these catalogues of star-forming galaxies to predict the CCSN discovery rate, primarily focused on low-metallicity events. In Section 2.3 a single 2.0-m telescope and

a network of 2.0-m telescopes (with limited observing time) are considered to perform a targeted CCSN survey of low-metallicity galaxies. In Section 2.4 the Panoramic Survey Telescope and Rapid Response System (Pan-STARRS) is considered to perform a dedicated, volume-limited CCSN survey and discovery rates are predicted for PS1 and PS4. Finally, in Section 2.5, all-sky transient surveys are considered to perform a dedicated, magnitude-limited CCSN survey and discovery rates are predicted for PS1, PS4 and the future LSST survey. Discussions and comparisons with other SN surveys are found in Section 2.6 and conclusions in Section 2.7.

2.2 Creating galaxy catalogues for various survey strategies

To produce the catalogues of galaxies that are to be used in conjunction with the various survey strategy simulations, we begin with the SDSS DR5 (see Section 1.5.1 and Adelman-McCarthy et al. 2007). To ensure that SNe discovered within the targeted and volume-limited surveys can be spectroscopically classified and monitored with relative ease they are required to be hosted by galaxies that are relatively nearby. To this end, a redshift-limit of $z = 0.04$ (~170 Mpc) is imposed on the SDSS spectroscopic table `SpecObjAll`. Within this redshift-limit there are 44,041 spectroscopically sampled galaxies within SDSS DR5. Data including the *ugriz* petrosian magnitudes, galactic extinction (from Schlegel et al. 1998), spectroscopic redshifts, *r*-band fibre magnitudes and emission-line intensities for each of the galaxies are extracted from the `SpecObjAll`, `SpecLineAll` and `PhotoObjAll` tables in the SDSS DR5 SQL server[1].

Two separate subsets of galaxies are drawn from this master set of 44,041 galaxies. The first of these subsets is classified as the *high signal-to-noise* (high-S/N) sample and contains galaxies with lines of Hα, Hβ, [O III]λ5007 and [N II]λ6584 detected above 7σ. The second sample is classified as the *low signal-to-noise* (low-S/N) sample, and contains galaxies *not* included in the high-S/N sample but exhibit lines of Hα and Hβ detected above 5σ. The high-S/N sample contains 20,632 galaxies and the low-S/N sample contains 8,703 galaxies. 14,706 galaxies remain unclassified as the lines of Hα and/or Hβ are not detected above 5σ.

2.2.1 Removing AGN host galaxies. To determine a core-collapse SN rate for each galaxy it is necessary to first determine their star-formation rates (see Section 2.2.3). The young, massive, hot stellar population within a galaxy provides a dominant source of hydrogen ionising radiation, making Hα luminosity a good SFR indicator. However, many of the galaxies within both the high- and low-S/N subsets play host to Active

[1] SDSS DR5 website: *http://www.sdss.org/dr5*

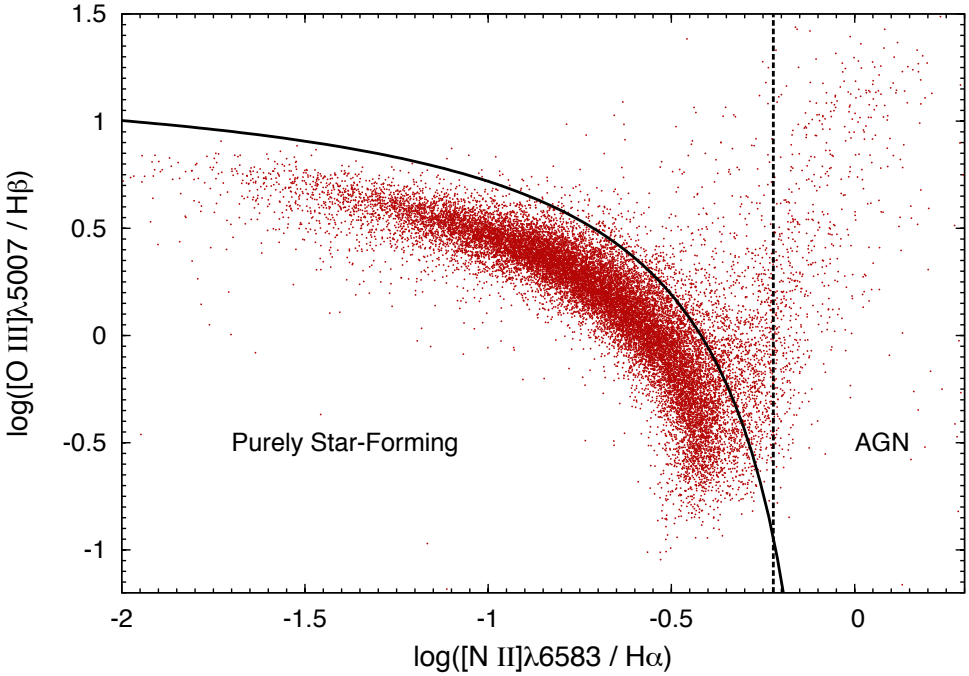

Figure 2.1: [O III]λ5007/Hβ vs [N II]λ6584/Hα plot for the 20,632 galaxies in the high-S/N subset. The diagnostic (solid) line from Kauffmann et al. (2003) discriminates between the purely star-forming galaxies (below line) and AGN host galaxies (above the line). The dashed line represents the division chosen for the star-forming galaxies and AGN for the low-S/N galaxy subset.

Galactic Nuclei (AGN). These AGN will also contribute to a galaxy's Hα luminosity. To remove these AGN contaminated galaxies from the high-S/N galaxy subset the following diagnostic line provided by Kauffmann et al. (2003) is used to discriminate between the purely star-forming galaxies (SFGs) and galaxies that host AGN:

$$\log\left(\frac{[\mathrm{OIII}]\lambda 5007}{\mathrm{H}\beta}\right) = \frac{0.61}{\log([\mathrm{NII}]\lambda 6584/\mathrm{H}\alpha) - 0.05} + 1.3 \qquad (2.1)$$

Figure 2.1 shows the SFGs found below this line and AGN host galaxies above the line. There are 18,350 high-S/N SFGs.

When considering the low-S/N galaxy subset, the spectral information provided is not accurate enough to apply this diagnostic line to remove AGN host galaxies. However, following the example of Brinchmann et al. (2004), it is still possible to remove the AGN hosts from the low-S/N subset by requiring that [NII]λ6584/Hα > 0.6 and that *nSigma* > 7σ in both lines. There are 6,000 low-S/N SFGs. An overview of the SDSS DR5 galaxies can be found in Table 2.1. The 14,706 unclassified galaxies are predominantly early-type galaxies that show little sign of recent star-formation and

All SDSS DR5 Galaxies [44,041]				
High-S/N [20,632]		Low-S/N [8,703]		Unclassified [14,706]
SFGs [18,350]	AGN [2,282]	SFGs [6,000]	AGN [2,703]	

Table 2.1: Hierarchy of galaxies drawn from a master set of SDSS DR5 spectroscopically sampled galaxies within $z = 0.04$.

hence Hα has not been detected to the significance levels required. A lack of recent star-formation within these galaxies implies that they will be void of any future CCSN events and therefore of little interest to a CCSN survey. Having removed all of the AGN contaminated galaxies, two catalogues of SFGs remain which shall henceforth be referred to as the high-S/N SFG (HSFG) catalogue and the low-S/N SFG (LSFG) catalogue.

2.2.2 Measuring the oxygen abundances. In order to flag low-metallicity galaxies from within the HSFG and LSFG catalogues, oxygen abundances are calculated using the calibration of Pettini and Pagel (2004), referred to from now on as PP04. The PP04 abundance indicator is empirically calibrated against the abundances of 137 extragalactic H II regions, all but 6 of which are measured via the electron temperature T_e method. To calculate the oxygen abundances of the SFGs within the range $8.12 \lesssim 12 + \log(\mathrm{O/H}) < 9.05$ the PP04 *O3N2* calibration is used:

$$12 + \log(\mathrm{O/H}) = 8.73 - 0.32 \log\left(\frac{[\mathrm{OIII}]\lambda 5007/\mathrm{H}\beta}{[\mathrm{NII}]\lambda 6584/\mathrm{H}\alpha}\right), \tag{2.2}$$

and below $12 + \log(\mathrm{O/H}) \simeq 8.12$ the PP04 *N2* calibration is used:

$$12 + \log(\mathrm{O/H}) = 8.9 + 0.59 \log([\mathrm{NII}]\lambda 6584/\mathrm{H}\alpha). \tag{2.3}$$

As the wavelengths of the emission-lines in the flux ratios of the PP04 calibration are separated by only a small amount the calibration is free from any extinction effects. Izotov et al. (2006) have measured oxygen abundances for 209 of the 18,350 HSFGs via the T_e method, often expressed as the most direct way to measure the abundance. For the majority of the 209 cross-matched galaxies, good agreement is found between the PP04 and the T_e abundances as expected. However, there are four outlying galaxies for which there is not good agreement (see Figure 2.2). These galaxies are SDSS J124813.65-031958.2, SDSS J091731.22+415936.8, SDSS J123139.98+035631.4 and

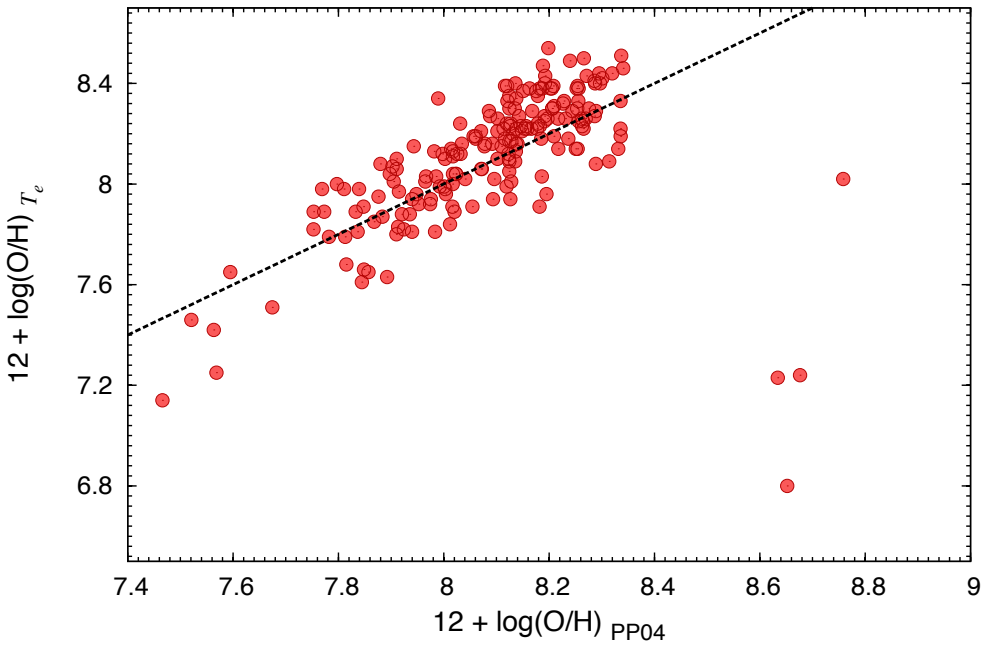

Figure 2.2: Comparing the PP04 empirically calibrated oxygen abundances with those directly measured by Izotov et al. (2006) via the electron temperature method reveals that the PP04 measurements are reliable, with an RMS scatter of 0.14 dex. The solid line shows a one-to-one correspondence. Note the four outlying galaxies - see text for details.

SDSS J130240.78+010426.8.

Examining the SDSS images of these four outlying galaxies reveals that they appear to be dwarf galaxies within the line-of-sight of, and possibly gravitationally bound to, much larger and presumably more metal-rich galaxies. Assuming that contamination from these background galaxies has not been adequately removed from the spectra of the dwarf galaxies by the SDSS reduction pipeline would explain the discrepancy between the oxygen abundances measured by Izotov et al. (2006) [2] and the PP04 abundances measured from the contaminated SDSS spectra. Due to contamination the oxygen abundances of a very small fraction of galaxies may be over-estimated. This is of little concern when aiming to produce a sample of low-metallicity galaxies as only a small fraction of galaxies will presumably fail to be flagged low-metallicity and will be excluded from the final sample. Choosing then to ignore these four outlying galaxies, the PP04 abundance measurements for the 205 remaining galaxies are found to fall with an RMS scatter of 0.14 dex from the T_e measured abundances. Examining SDSS

[2]Izotov et al. (2006) manually measured the individual emission-line fluxes from the SDSS spectra using the IRAF SPLOT tool.

images of a random selection of these remaining galaxies from the Izotov et al. (2006) sample reveal the blue compact dwarf galaxies expected from their low-metallicity sample.

Recently Prieto et al. (2008) have taken a sample of 125,958 SFGs from SDSS DR4, with oxygen abundances measured in the same fashion as Tremonti et al. (2004), derived via a likelihood analysis which simultaneously fits multiple optical, nebular, emission-lines to those predicted by the hybrid stellar-population plus photoionisation models of Charlot et al. (2002). A likelihood distribution of metallicity is determined for each galaxy and the median is taken as the best estimate of the galaxy metallicity. These metallicities are essentially on the Kewley and Dopita (2002) abundance scale. Cross-matching the catalogues of HSFGs and LSFGs against the Prieto et al. (2008) sample produces a common sample of 18,014 galaxies. The PP04 oxygen abundances are found to be typically ~0.2 dex below these measured on the Kewley and Dopita (2002) scale, in agreement with the findings of Modjaz et al. (2008). The cause of this discrepancy is debated and may be due either to (*a*) certain parameters that produce temperature variations not being taken into consideration when deriving T_e at higher-metallicities leading to an under-estimation of the PP04 oxygen abundances (Stasińska 2005; Bresolin 2006), or (*b*) an unknown problem with the photoionisation models used by Tremonti et al. (2004) (see Kennicutt et al. 2003).

2.2.3 Core-collapse supernova rates. Having measured the oxygen abundance of each galaxy in the HSFG and LSFG catalogues, the core-collapse supernova rates (CCSRs) now have to be determined. To do this galaxy star-formation rates (SFRs) must first be measured and then the fraction of these stars that will eventually end their lives as CCSNe must be determined. The best indicator available for SFR is Hα luminosity. As alluded to previously, the young, massive, hot stellar population is the dominant source of hydrogen ionising radiation in purely star-forming galaxies, causing a galaxy's Hα luminosity to be proportional to its recent SFR. Kennicutt (1998) has determined the following calibration between SFR and Hα luminosity:

$$\mathrm{SFR}_{\mathrm{H}\alpha}(\mathrm{M}_{\odot}\ \mathrm{yr}^{-1}) = \frac{L_{\mathrm{H}\alpha}}{1.27\times10^{34}} \tag{2.4}$$

where the luminosity is measured in Watts.

Derived from model fits, Brinchmann et al. (2004) also provide likelihood distributions for the conversion factor between the Hα luminosity and SFR for galaxies of various mass ranges. They confirm that the Kennicutt calibration is a good *typical* calibration, comparing well with the median value for their sample. When considering

the complete HSFG and LSFG catalogues it is acceptable to assume a median mass range for the galaxies and the Kennicutt calibration is employed. However, a sample of moderately low-metallicity galaxies is best represented by the Brinchmann et al. (2004) distribution with the lowest mass range ($\log M_* < 8$) as these galaxies are typically low-mass, dwarf galaxies:

$$\mathrm{SFR}_{\mathrm{H}\alpha}(\mathrm{M}_\odot\ \mathrm{yr}^{-1}) = \frac{L_{\mathrm{H}\alpha}}{2.01 \times 10^{34}} \tag{2.5}$$

SDSS provides the Hα equivalent line width and also the continuum flux at the wavelength of Hα. The equivalent width times the continuum flux gives the Hα flux which is then used to determine the Hα luminosity. A problem associated with the SDSS data is that only that flux which falls within the 3″ fibre aperture of the SDSS multi-fibre spectrograph is measured. Typically this is only a fraction of the total galaxy flux, as the SDSS spectrograph fibre locks onto the centre of the galaxy and any flux that falls outside of the 3″ fibre aperture is lost. Hopkins et al. (2003) have developed a very simple aperture-correction that can be applied to the measured galaxy Hα luminosity to give an estimate of the total galaxy Hα luminosity. This aperture-correction takes account of the ratio between the petrosian photometric r-band galaxy magnitude and the synthetic r-band fibre magnitude determined from the galaxy spectrum. Hopkins et al. (2003) also provide an extinction correction to be used when determining the galaxy Hα SFR, which makes use of the Balmer decrement and assumes the standard Galactic extinction law of Cardelli et al. (1989). The final aperture and extinction corrected Hα luminosity SFR indicator to be used with the HSFG and LSFG catalogues is:

$$\mathrm{SFR}_{\mathrm{H}\alpha}(\mathrm{M}_\odot\ \mathrm{yr}^{-1}) = 10^{-0.4(r_{\mathrm{Petro}} - r_{\mathrm{fibre}})} \left[\frac{S_{\mathrm{H}\alpha}/S_{\mathrm{H}\beta}}{2.86} \right]^{2.114} \frac{L_{\mathrm{H}\alpha}}{1.27 \times 10^{34}} \tag{2.6}$$

and for low-metallicity sub-samples:

$$\mathrm{SFR}_{\mathrm{H}\alpha}(\mathrm{M}_\odot\ \mathrm{yr}^{-1}) = 10^{-0.4(r_{\mathrm{Petro}} - r_{\mathrm{fibre}})} \left[\frac{S_{\mathrm{H}\alpha}/S_{\mathrm{H}\beta}}{2.86} \right]^{2.114} \frac{L_{\mathrm{H}\alpha}}{2.01 \times 10^{34}} \tag{2.7}$$

where $S_{\mathrm{H}\alpha}$ and $S_{\mathrm{H}\beta}$ are the line fluxes corrected for stellar absorption (according to Hopkins et al. 2003).

Figure 2.3 compares the measured SFRs with oxygen abundance. In general a higher SFR is associated with a higher oxygen abundance. It can be argued that if the SFR of a galaxy is high, or has been high at any point in its history, then the increased population of young, hot, massive stars will have led to an increased CCSR and therefore a greater rate of enrichment of the ISM. The observed high-metallicity cutoff of the SDSS galaxies seen in Figure 2.3 is probably due to a saturation suffered by [O

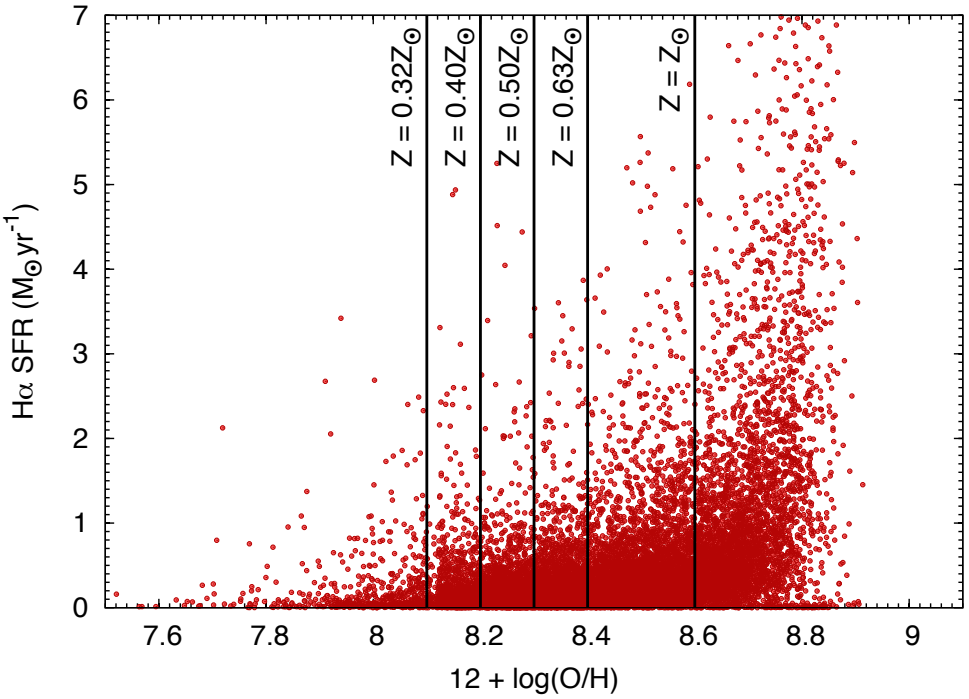

Figure 2.3: Hα determined star-formation rates using the low-mass range calibration of Brinchmann et al. (2004) for the 18,350 HSFGs compared with their measured oxygen abundances. In general a higher metallicity is accompanied by a higher star-formation rate, as expected.

III] λ4363 in the T_e calibrated metallicities (see Kewley and Ellison 2008).

Given a SFR, it is relatively simple to convert to a CCSR by determining the fraction of the stellar population that will eventually end their lives as CCSNe. Following the method used by *e.g.* Mattila and Meikle (2001), the initial mass function (IMF) is used to calculate the fraction of a stellar population within the mass range $8M_\odot < M < 50M_\odot$, the range predicted for stars to end their lives as CCSNe. From this logic the CCSR is determined as:

$$\mathrm{CCSR} = \frac{\int_{8M_\odot}^{50M_\odot} \phi(m)dm}{\int_{0.1M_\odot}^{125M_\odot} m\phi(m)dm} \times \mathrm{SFR} \tag{2.8}$$

where $\phi(m)$ is the Salpeter IMF (Salpeter 1955) with upper and lower mass cut-offs of $0.1M_\odot$ and $125M_\odot$. This conversion is calculated to be:

$$\mathrm{CCSR(SNe\ yr^{-1})} = 0.007 \times \mathrm{SFR}(M_\odot\ \mathrm{yr}^{-1}) \tag{2.9}$$

HSFG Catalogue

	INDIVIDUAL GALAXY SN RATE LIMITS					
	> 0.0 SNe yr^{-1}		> 0.001 SNe yr^{-1}		> 0.01 SNe yr^{-1}	
12+log(O/H)	Galaxies	SNe yr^{-1}	Galaxies	SNe yr^{-1}	Galaxies	SNe yr^{-1}
No Limit	18,350	115.6	13,974	113.4	2,557	73.6
< 8.4	8,019	13.2	3,650	11.2	120	2.3
< 8.3	4,290	6.9	1,830	5.9	73	1.3
< 8.2	1,713	3.1	**727**	**2.8**	42	0.8
< 8.1	537	1.0	209	0.9	16	0.3

LSFG Catalogue

	INDIVIDUAL GALAXY SN RATE LIMITS					
	> 0.0 SNe yr^{-1}		> 0.001 SNe yr^{-1}		> 0.01 SNe yr^{-1}	
12+log(O/H)	Galaxies	SNe yr^{-1}	Galaxies	SNe yr^{-1}	Galaxies	SNe yr^{-1}
No Limit	6,000	34.1	3,691	33.2	901	22.9
< 8.4	1,757	0.8	116	0.3	6	0.1
< 8.3	1,025	0.3	50	0.1	0	0.0
< 8.2	401	0.1	18	0.0	0	0.0
< 8.1	116	0.0	4	0.0	0	0.0

Nearby Bright Galaxy Catalogue

Galaxies	SNe yr^{-1}
1,216	12.70

Table 2.2: The table shows the expected CCSN rates within the SDSS DR5 spectroscopic survey area (14% of the entire sky) out to a redshift of $z \sim 0.04$.

2.2.4 Additional nearby bright galaxies. To avoid saturation and excessive cross-talk in the spectrographs, target selection criteria for the SDSS DR5 spectroscopic sample includes a bright magnitude limit of $r \sim 14.5$. As a result of this restriction many nearby luminous galaxies have been omitted from the DR5 spectroscopic sample. To account for these missing bright galaxies, galaxies from the HyperLeda extragalactic database[3] are cross-matched against galaxies from the SDSS DR5 `PhotoObjAll` table with magnitudes $r < 14.5$. From this cross-matched selection of galaxies, those galaxies *not* found in the SDSS DR5 `SpecObjAll` table are extracted. This selection produced a total of 1,887 nearby luminous galaxies that are included in the SDSS DR5 photometric survey but omitted from the spectroscopic survey.

It is necessary to know what fraction of these 1,887 galaxies are star-forming. HyperLeda provides a galaxy morphological classification for a large number of the galaxies in its database making it possible to remove all galaxies with an early-type classification, as these galaxies will generally have very low SFRs[4]. The mean $g-i$ colour of

[3] http://leda.univ-lyon1.fr

[4] Note however that some early-type galaxies have H II regions and some evidence of low-level star-

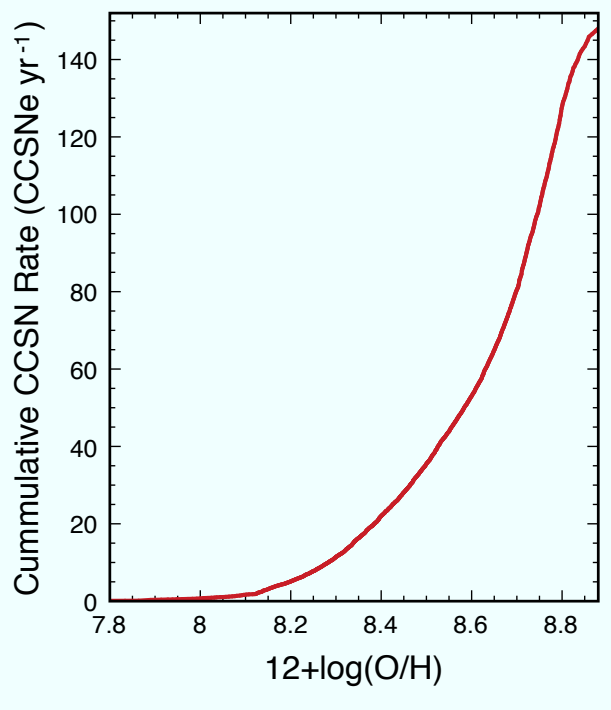

Figure 2.4: Cumulative distribution of the combined CCSN rate from the HSFG and LSFG catalogues, measured against oxygen abundance. It is clear that as oxygen abundance increases so to does the rate of CCSNe

these early-type galaxies is 1.216, with standard deviation $\sigma = 0.153$. In an attempt to remove the remaining non-SFGs with no morphological classification from this bright galaxy selection, all galaxies redward of one σ from the mean $g-i$ colour are removed, i.e. $g-i > 1.063$. 1,216 SFGs remain. There is a possibility that a few heavily reddened starburst galaxies may have been excluded from this selection, but this is of little concern when primarily considering low-metallicity galaxies which are generally not greatly affected by extinction.

These nearby bright SFGs have no associated spectral information, therefore it is necessary to use an alternative indicator to estimate SFR other than Hα. It is possible to use the U-band luminosity as an alternative SFR indicator using the relationship developed by Moustakas et al. (2006):

$$\mathrm{SFR}_{U_{obs}}(\mathrm{M}_{\odot}\mathrm{yr}^{-1}) = (1.4 \pm 1.1) \times 10^{-43} \frac{L_{U_{obs}}}{\mathrm{ergs\ s}^{-1}}, \tag{2.10}$$

converting the SDSS u-band to U_{vega} using the following transformation from Blanton and Roweis (2007):

$$U_{\mathrm{vega}} = u - 0.0140(u-g) + 0.0556, \tag{2.11}$$

formation (e.g. Moss and Whittle 2005).

and using distance moduli from HyperLeda determine $L_{U_{obs}}$. As Moustakas et al. (2006) have empirically calibrated this U-band SFR indicator from extinction-corrected Hα galaxy luminosities, there is no need to further correct this indicator for dust reddening. The CCSR is then determined using Equation 2.9. The 1,216 additional nearby bright galaxies have a resulting U-band indicated CCSR of 12.70 CCSNe yr^{-1}.

In summary, there are now three galaxy catalogues with estimated CCSRs; the HSFG and LSFG catalogues and an additional SFG catalogue. Taking the 18,350 HSFGs and the 6,000 LSFGs and introducing various upper-limits to the metallicity and lower-limits to the CCSRs it is possible to define separate sub-samples of galaxies. Table 2.2 displays these sub-samples, differing both in the number of galaxies they contain and their estimated cumulative CCSR. For samples of galaxies with no metallicity constraint, the SFRs have been derived using the 'typical' calibration of Kennicutt (1998). For the sub-samples of galaxies with metallicity constraints the SFRs have been derived using the lowest mass range calibration of Brinchmann et al. (2004). Figure 2.4 shows a cumulative distribution of the HSFG and LSFG catalogued CCSR measured against oxygen abundance. It is clear that the CCSR increases steeply with oxygen abundance.

With an idea of the total rate of CCSNe hosted within the local universe, it is now possible to estimate the CCSN discovery rates for various survey strategies by predicting their detection efficiency through detailed survey simulations.

2.3 Survey Strategy 1: A targeted survey of catalogued low-metallicity galaxies

The first survey strategy to be considered uses (*a*) a single 2.0-m telescope and (*b*) a network of 2.0-m telescopes to target a limited number of low-metallicity galaxies to search for CCSNe. The fully robotic 2.0-m Liverpool Telescope situated at the Observatorio del Roque de los Muchachos, La Palma is considered as the prototypical, single 2.0-m telescope. To gain access to the 2.0-m telescopes required to operate this survey strategy it will be necessary to apply for observing time via the appropriate channels. As this process is highly competitive, this survey strategy shall be restricted by limited observing time.

Three characteristics are required of the galaxy catalogue to be used in conjunction with this strategy. Firstly, the catalogue must contain only a few hundred galaxies, otherwise if the catalogue is too large each individual galaxy will not be observed frequently enough to ensure the detection any SNe that it may host. Secondly, the catalogued galaxies are required to be of sufficiently low metallicity. Finally, the catalogued galaxies must exhibit a suitably high CCSR to optimise the probability of detecting CC-

SN Type	Number	Relative Rate	Core-Collapse Only
Ia	25	24.8%	-
IIP	43	42.6%	56.6%
IIL	2.5	2.4%	3.3%
Ibc	28	27.7%	36.6%
IIn/P	1.25	1.2%	1.6%
IIn/L	1.25	1.2%	1.6%

Table 2.3: Relative CCSRs included in the survey simulations. Rates are taken from a draft of Smartt et al. (2009) and vary a little from the published rates.

SNe. The latter two requirements somewhat contradict each other as metallicity tends to scale with SFR; requiring galaxies with low-metallicity typically restricts us to galaxies with lower SFRs, and hence lower CCSRs. It is therefore essential to produce a galaxy catalogue that can act as a compromise between these two conflicting requirements.

A galaxy catalogue that optimally fits the requirements of this survey strategy is the sub-sample of the HSFG catalogue that contain galaxies with oxygen abundances less than 8.2 dex and a CCSR greater than 1.0 CCSNe every 1,000 years (highlighted in Table 2.2). This low-metallicity catalogue contains 727 galaxies, a suitable number for a targeted survey, with an estimated CCSR of 2.8 CCSNe yr^{-1}. This galaxy catalogue is extracted from the SDSS DR5 spectroscopic survey footprint; 5,713 square degrees, *i.e.* 14% of the entire sky. It can be assumed that the rest of the sky contains similar density of these low-metallicity galaxies. We shall return to this point later. Due to the practical limiting factors of a targeted survey strategy, it shall only be possible to detect a fraction of the estimated 2.8 CCSNe yr^{-1} that this low-metallicity galaxy catalogue will harbour. A simulation of the survey strategy is created to estimate this factor.

2.3.1 Survey simulation parameters. **Supernova rates:** To accurately reproduce the relative rates of CCSN types, the observed rates compiled by Smartt et al. (2009) are ingested into the simulation (Table 2.3). These rates have been compiled from a time and volume-limited sample, accounting for all SNe discovered within the eight year period between 1999 January 1 and 2006 December 2006 in galaxies with a recessional velocity $< 2{,}000 kms^{-1}$. Apart from those SNe that inhabit environments of heavy extinction, it is assumed that within this appointed distance limit ($\mu = 32.3$) that all SNe should have been bright enough to have been discovered and that these rates are relatively free from Malmquist bias. SNe Type IIb are included under Type Ibc, and SNe Type IIn have been divided evenly between those with a plateau phase (IIn/P) and those with a linear phase (IIn/L) in the tail of their lightcurves.

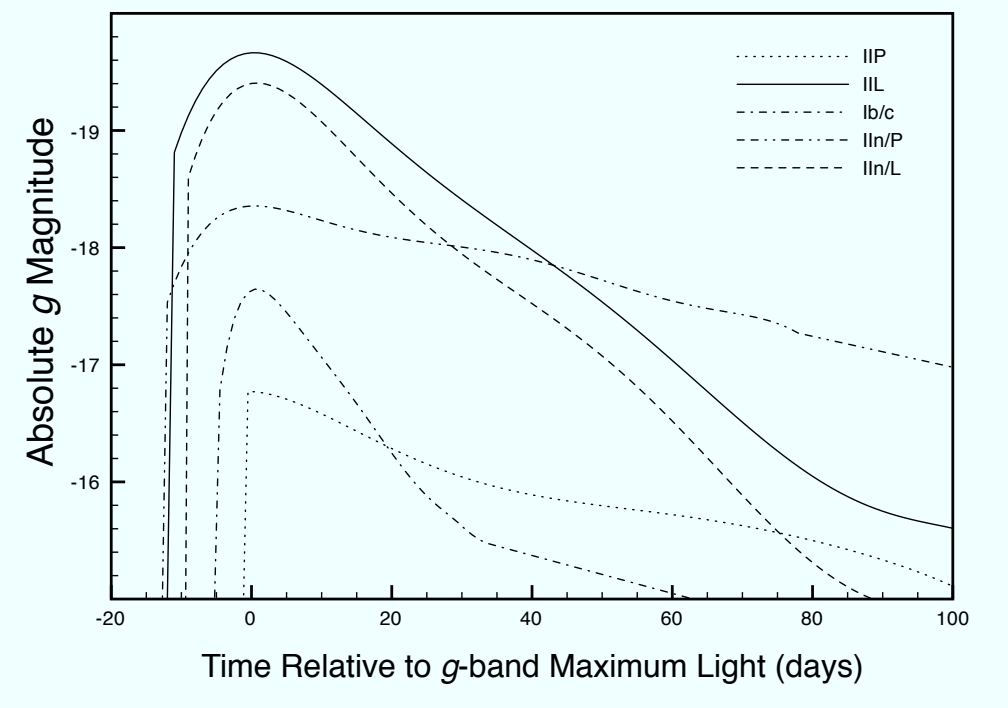

Figure 2.5: Template lightcurves used within the Monte-Carlo simulation. Lightcurve for SNe Type IIP from SN 1999em, Type IIL from SN 1998S, Type Ibc from SN 2002ap, Type IIn/P from 1994Y and Type IIn/L from SN 1999el. Note that all magnitudes are in the AB system.

Template lightcurves: Template lightcurves of the various CCSNe Types are also included in the simulation (see Fig 2.5). SN 1999em is used as the Type IIP template with data taken from Hamuy et al. (2001). SN 1998S is used as a template for Type IIL taking data for the rise to maximum light from Liu et al. (2000) and data for the tail from Fassia et al. (2000). SN 2002ap is used as a template for Type Ibc with data taken from Foley et al. (2003). SN 1994Y is used as a template for Type IIn/P with data taken from Ho et al. (2001), allowing SN 1998S to provide the rise to maximum light. SN 1999el is used as the template for Type IIn/L taking data from Carlo et al. (2002), again allowing 1998S to provide the rise to maximum light. The following transformation from Blanton and Roweis (2007) is used to convert all lightcurve data to the *g*-band (AB magnitudes):

$$g = B - 0.03517 - 0.3411(B - V) \tag{2.12}$$

Peak magnitude distribution: The absolute magnitude distributions of Richardson et al. (2002) are included in the simulation to provide accurate weightings to the peak magnitudes of the simulated SNe (Table 2.4). Equation 2.12 is used to transform these distributions to the *g*-band taking the $(B-V)$ colour from the epoch of peak *g*-

SN Type	M_B	M_g	σ
IIP	-17.00	-17.02	1.12
IIL	-18.03	-18.00	0.90
Ib/c	-18.04	-18.22	1.39
IIn/P	-19.15	-19.24	0.92
IIn/L	-19.15	-19.24	0.92

Table 2.4: Peak magnitude distributions from Richardson et al. (2002). σ is the range in the peak magnitude distribution and *g*-band magnitudes are given in the AB system.

magnitude from our template lightcurves. When choosing a filter with which to perform a SN search with the Liverpool Telescope the *r*-band is superior to the *g*-band as it has a greater filter throughput, the CCD detector is more responsive in the red and also SNe are generally brighter in the *r*-band, especially later in their evolution. However, the Richardson et al. (2002) distributions of SN peak magnitudes are given in the *B*-band which can be transformed to the *g*-band but not the *r*-band. For this reason a *g*-band survey is simulated and the results extrapolated to the *r*-band.

Distance and extiction: The final two parameters incorporated into the simulation are the host galaxy distances and the extinction toward the SNe. A random distance is assigned to each host galaxy, out to the distance limit of the survey ($z = 0.04$), assuming that the galaxies included in the survey are spread homogeneously and isotropically throughout the survey volume. Considering that the majority, if not all, of the galaxies within the catalogue are low-luminosity, blue, dwarf galaxies with relatively low metallicities, it can be assumed that host galaxies will suffer from little internal extinction. Therefore only a typical Galactic extinction is assigned to each SN ($A_g = 0.3$).

Cadence: A major factor influencing the detection efficiency of any SN survey is the time between consecutive observations of a galaxy hosting a SN. As this time increases, so too does the likelihood that the SN will not be observed until it is well advanced in its lightcurve evolution. This could result in the magnitude of the SN dropping below the detection limit of the survey and hence failing to be detected. There are three parameters that affect the survey cadence which are addressed by the simulation. The first of these is the probability that a SN will be in solar conjunction for a fraction, if not all, of the time it remains detectable by the survey. To account for this factor, the celestial coordinates of the 727 catalogued low-metallicity galaxies and an almanac for the Liverpool Telescope are used to produce a distribution of the fractions of the year that these galaxies are observable. This distribution has a mean fraction of 0.38 and is incorporated into the simulation to account for cases where a SN would be

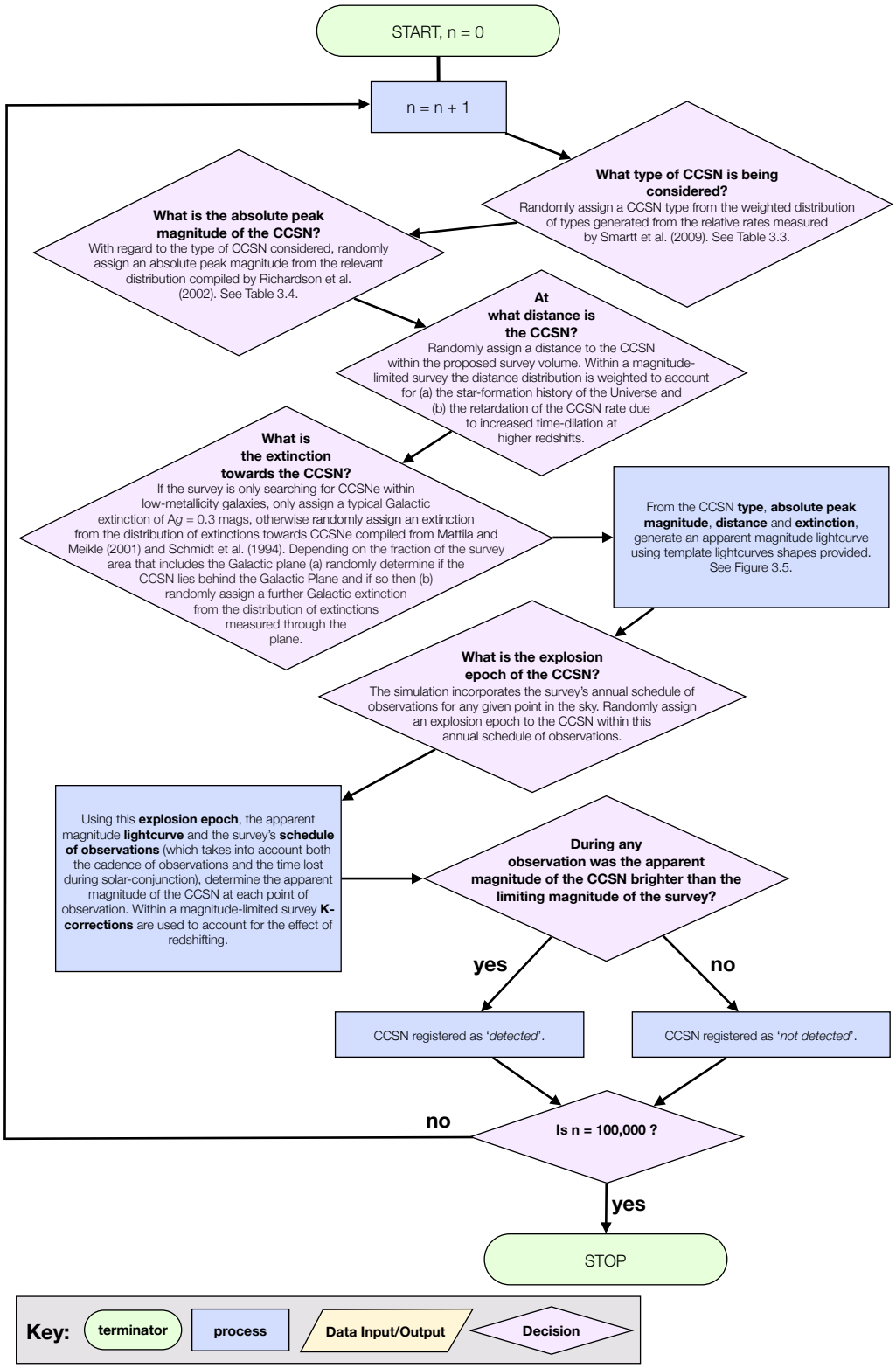

Figure 2.6: Schematic workflow of the Monte Carlo Simulations used to predict the fraction of CCSNe that will be detected using various survey strategies. Given survey specific parameters, such as limiting magnitudes and the cadence of observations, the simulation randomly generates 100,000 CCSNe within the survey volume and determines whether or not they would be detected by the survey.

unobservable, and hence undetectable, because its host galaxy is behind the sun.

The second factor that affects the cadence is the fraction of time that cannot be used by the Liverpool Telescope to perform the survey. Reasons why the telescope could not be used on any particular night include weather, technical difficulties and scheduled maintenance nights. To account for this unusable time, nightly reports from 2005 August 1^{st} to 2006 July 31^{st} are taken from the Liverpool Telescope website[5] and are used to determine an annual distribution of nights (58% of nights in total) that can be used for our search. This distribution of usable nights is incorporated into the simulation.

The final factor that will affect the cadence of observations, is the number of galaxies targeted every night. This number is influenced by the amount of telescope time dedicated each night to the survey; the greater the amount of time, the greater the number of galaxies observed per night and the higher the cadence of observations. The number of galaxies that can be observed each night is also affected by image exposure time. Increasing the exposure time increases the depth of the survey, meaning that fainter SNe are detectable and SNe are detectable for a greater period of time. By running the simulation multiple times for (*a*) a varying number of hours/night that the LT dedicates to the survey and (*b*) varying image exposure time, an optimal balance between these parameters can be derived that shall ensure detection of the greatest fraction of the CCSNe predicted from low-metallicity galaxy catalogue. The results can be seen in Fig. 2.7.

Results of these simulations suggest that the small difference between the percentage of CCSNe detected while observing one hour as opposed to two hours per night or more is not enough to justify the extra observing time. Note that the detection rates are double valued either side of the peak rate. As it is favourable to detect SNe earlier in their evolution, a shorter image exposure time should be chosen as this increases the cadence of observation and thereby increase the probability of discovering CCSNe earlier.

2.3.2 Predicted discovery rates for a single 2.0m telescope. The survey simulation is triggered to randomly generate 100,000 SNe within the survey volume. The information gained about each SN generated by the simulation include its apparent magnitude at the point of observation. Only if this magnitude is above the limiting-magnitude of the survey is a SN is registered as being discovered.

[5]LT website: *http://telescope.livjm.ac.uk/*

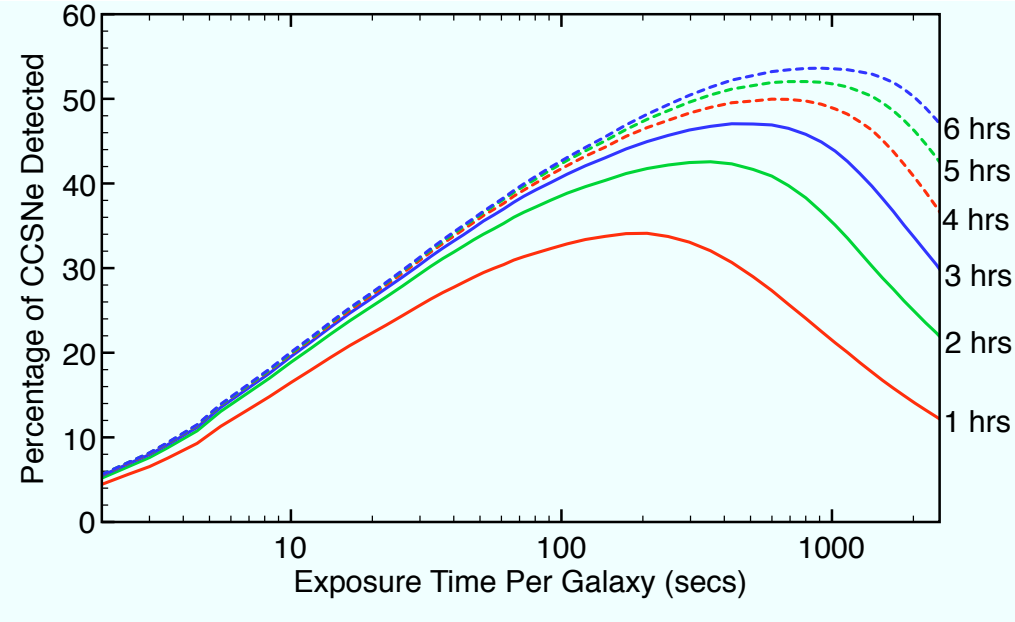

Figure 2.7: Percentage of CCSNe discovered by a targeted survey for a differing number of hours observing per night (labeled to the right of the plot). The percentage of CCSNe discovered increases as nightly observing time increases, as this increases the cadence of observations. As the image exposure time increases, the limiting-magnitude of the survey deepens but the cadence of observations decreases. There is therefore an optimal point at which the exposure time and cadence of observation are balanced to discover a maximum percentage of SNe.

Aiming to observe one hour per night using 60 sec exposures allows each galaxy to be observed once every ~17 days (see Figure 2.7). Using the g-band, 29.6% of CCSNe are predicted to be discovered with this survey strategy. This equates to a detection of 0.8 of the 2.8 CCSNe yr^{-1} predicted from the catalogue of 727 low-metallicity galaxies and a total of 154 hrs yr^{-1} of 2.0-m telescope time. Given a 60 sec exposure the AB limiting magnitudes for the Liverpool telescope are $g = 18.7$ and $r = 19.0$. With this survey strategy a typical SN will be observed ~73 days post-explosion with $g - r = 0.8$ mags. Given the difference in limiting magnitudes and the typical $g - r$ colour at the point of observation, SNe ~1.1 magnitudes fainter than the limit of a g-band survey shall be detected in an r-band survey. Assuming that the template lightcurves and the distribution of SN peak magnitudes are similar in the r-band compared to the g-band, the g-band simulation is re-run with a limiting magnitude 1.1 magnitudes fainter than previously used. From this pseudo r-band simulation it is predicted that 47.8% of CCSNe will be discovered. This equates to a detection of 1.3 of the 2.8 CCSNe yr^{-1} predicted from the catalogue of 727 low-metallicity galaxies. Assuming a typical Galactic extinction of $A_g = 0.3$ ($A_r = 0.22$) and an exposure time of 60 seconds the estimated absolute limiting magnitude (25σ significance) for this survey will be $M_r = -12.7$ at a distance of

20Mpc, $M_r = -15.4$ at 70Mpc and $M_r = -17.1$ at 150Mpc.

Limiting magnitudes of a relatively high significance level (25σ) are required of all of the survey strategies considered throughout this chapter. The image matching and subtraction method (see Alard and Lupton 1998) shall be used to detect SNe. Assuming that the original images have equal depths, this process of image subtraction increases the noise by roughly a factor of $\sqrt{2}$ so that the relative significance level of the limiting magnitude of the differenced image is reduced to $\sim 18\sigma$. In addition, the detection of SNe inside their host galaxies will be always more difficult due to image subtraction residuals caused by uncertainties in the alignment and matching of two images. Without these high significance limiting magnitudes the large count of spurious detections would result in huge numbers of false SN candidates to be humanly inspected. For the strategies considered with dedicated all-sky surveys (Sections 2.4 and 2.5) these numbers could range into the hundreds of thousands every night. A finely tuned transient classification pipeline may help to automatically reject a large fraction of these spurious detections so that the signicance levels of the limiting magnitudes can be reduced. This would result in a larger number of SNe being discovered and also many SNe being discovered earlier in thier evolution.

2.3.3 Predicted discovery rates for a network of 2.0m telescopes. As previously discussed, SDSS DR5 covers ~14% of the entire sky. If it were possible to compile a catalogue of low-metallicity galaxies for the whole sky and use a network of seven 2.0-m telescopes (or three to four 2.0m telescopes with double the time allocation) to survey these galaxies then we should expect to discover roughly 7 times the CCSNe detected by a single 2.0-m telescope, *i.e.* ~9.3 CCSNe yr^{-1}. A network similar to the RoboNet[6] global network of 2.0-m telescopes consisting of the LT and the Faulkes Telescopes North and South could be considered to perform this kind of survey. An advantage of using a network of telescopes in both the northern and southern hemispheres is the gain in sky coverage which allows for a greater number of galaxies to be targeted by the survey.

The two obstacles that would be encounter with this survey strategy are (*a*) the generous amount of telescope required (~1,000 hrs yr^{-1}) and (*b*) the present lack of data required to compile an all-sky galaxy catalogue. Compiling a catalogue of all known galaxies listed in the 2dF, 6dF, LEDA and SDSS DR5 within the limit z<0.04 results in a catalogue of 103,549 individual galaxies, a fraction of which are star-forming. PS1, the prototype 1.8-m survey telescope of the Panoramic Survey Telescope and Rapid Response System (Pan-STARRS) shall survey 3π of the sky to a depth exceeding that

[6] http://www.astro.ljmu.ac.uk/RoboNet/

of SDSS DR5 enabling the compilation of a relatively complete nearby low-metallicity galaxy catalogue covering $\sim 3/4$ of the sky.

2.4 Survey Strategy 2: A volume-limited search with the Pan-STARRS all-sky survey

Having considered a targeted low-metallicity galaxy survey to search for CCSNe both with a single and a network of 2.0m telescopes, attention is now given to the Pan-STARRS all-sky survey (see Section 1.5.2). As this is an all-sky survey, the galaxy catalogue to be used in conjunction with the survey no longer has to be limited; all galaxies within the HSFG, LSFG and addition bright galaxy catalogues will automatically be observed. Also, as Pan-STARRS is a *dedicated* survey, access to the telescope is unrestricted. This is a huge advantage over using a single or a network of 2.0m telescopes where only limited access may be granted via a highly competitive application process.

2.4.1 Survey simulation parameters. The simulation of the volume-limit survey strategy uses many of the same parameters detailed for the targeted survey (Section 2.3.1). The adapted parameters are as follows.

Cadence: Of all the modes in which PS1 shall be run the 3π Steradian Survey (covering 30,000 square degrees of the sky) shall be the most effective when searching for CCSNe. The survey aims to cover that whole sky 60 times in 3 years; 12 times in each of the *grizy* filters. These timescales have taken historic weather patterns on Haleakala into consideration. This simulation incorporates the cadence of the PS1 survey strategy (Chambers 2007), see Figure 2.8. The survey has a predicted AB limiting magnitudes (25σ) of $g = 21.5$ and $r = 20.9$ mags and for single 60 second and 38 second exposures respectively (Chambers 2007). Assuming a typical Galactic extinction of $A_g = 0.3$ ($A_r = 0.22$), the estimated absolute limiting magnitudes (25σ significance) for this survey will be $M_g = -14.7$ and $M_r = -15.2$ at a distance of 150Mpc.

Limiting magnitude: It is assumed that the fraction of CCSNe discovered in the g-band can be taken as the typical fraction that will be detected in each of the *grizy* filters; indeed running the magnitude-limited survey simulation (detailed in Section 2.5.1) in an attempt to predict the CCSN discovery rate of this simulated survey using all five filters, where the K-corrections essentially behave as colour corrections at such low redshift, results in predicted detection efficiencies extremely close to those found if considering only the g-band. Simulating a PS1 volume-limited survey will again

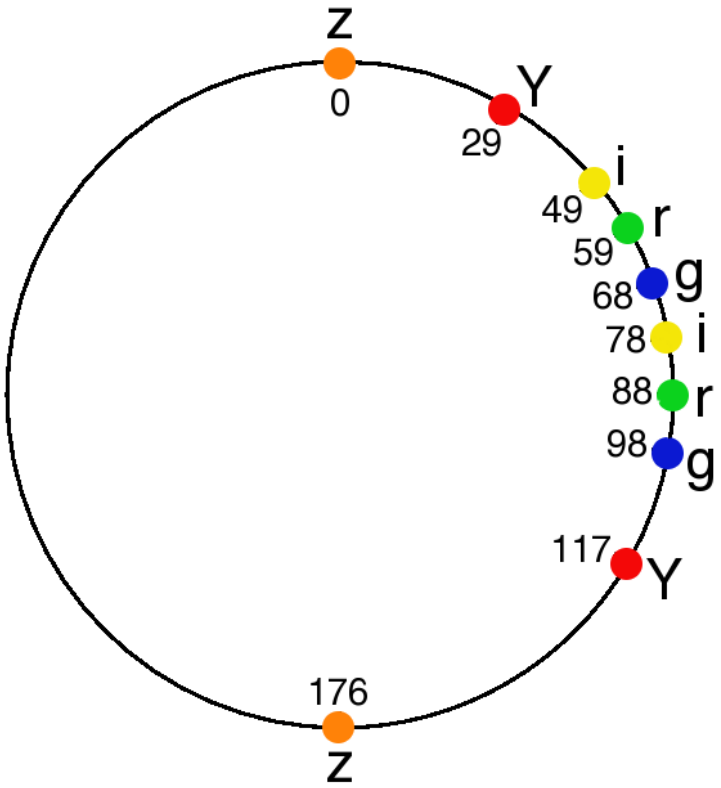

Figure 2.8: A schematic depicting the cadence of observation for any given point in the sky, taken from the Pan-STARRS observation strategy (Chambers 2007). One Pan-STARRS year of 12 lunar months, approximately 352 days, is represented by the circle. With each observation epoch a double exposure is taken in order to identify Near Earth Objects and fast-transients.

help to estimate the fraction of CCSNe that will actually be detected with the survey strategy.

Extinction: When considering a simulated survey of the *all* of the catalogued SFGs (*i.e.* a search for *all* SNe within the assigned survey volume), a random extinction is assigned to each of the CCSNe using a weighted distribution based on CCSRs taken from Mattila and Meikle (2001) and Schmidt et al. (1994). However, when simulating a survey restricted to low-metallicity galaxies (≤8.2 dex) only a typical Galactic extinction of $A_g = 0.3$ is assigned to the CCSNe, as at these metallicities the galaxies are expected to be relatively dust free.

A fraction of SNe remain undetected within spiral galaxies that are not observed face on (e.g. Cappellaro et al. 2003) as the average extinction attributed to SNe in spiral galaxies with higher inclination angles is higher than that of face on spiral galaxies, making the SNe fainter and more difficult to detect. Implementing a correction

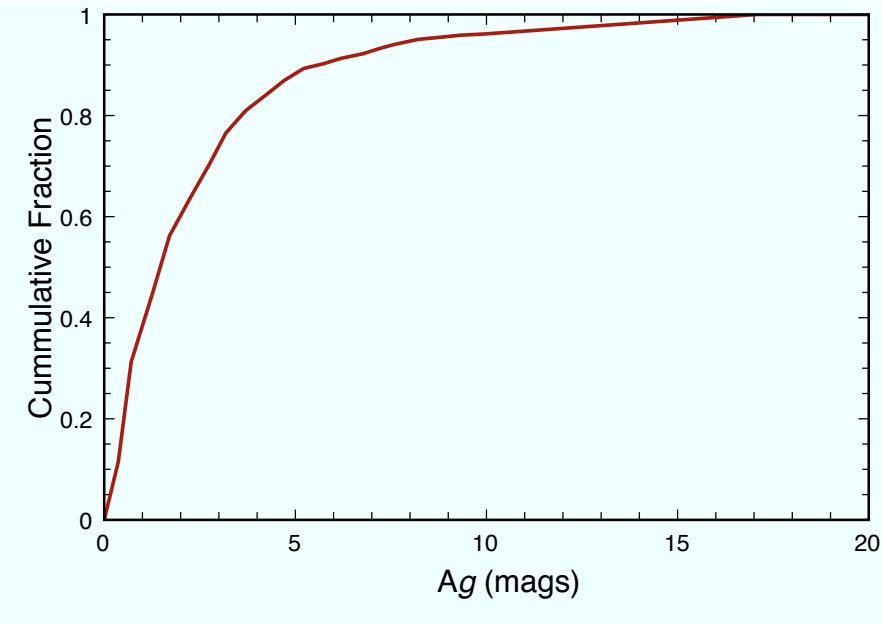

Figure 2.9: Cumulative distribution of the extinctions measured at ~1,500 points in the Galactic Plane within the Pan-STARRS survey area.

for this effect in the survey simulations, using a similar method to that of Riello and Patat (2005), could easily result in an under-estimation of the CCSRs observed in low-metallicity galaxies as these tend not be to grand-design spiral galaxies but rather dwarf, irregular galaxies where the effect of galaxy inclination would be negligible. An attempt to correct for this effect is therefore not included in the simulations which may make the predictions of the SN discovery rates in the full galaxy catalogues with no metallicity limit somewhat optimistic. This should not be a significant over-estimation of events, as the SFRs calculated come from the observed galaxy Hα luminosities which will also be lower in inclined spirals than in face on targets.

The Pan-STARRS survey area covers a large fraction of the sky that is obscured by the Galactic Plane, a total of ~7,500 square degrees. SNe located behind the Galactic Plane shall be extinguished above a typical Galactic extinction. To account for this excess extinction in the survey simulations, ~1,500 points positioned homogeneously across the expanse of the Galactic Plane within the Pan-STARRS area are used to produce a distribution of extinction (Schlegel et al. 1998). This distribution is used to accurately simulate the extinction assigned to any SNe that fall behind the Galactic Plane. The cumulative distribution of these extinctions can be found in Figure 2.9.

2.4.2 Predicted discovery rates for PS1. A PS1 volume-limited survey of galaxies (within $z \leq 0.04$) is predicted to discover 66.9% of all CCSNe, and a survey of lower

metallicity galaxies is predicted to discover 74.2% of CCSNe. The predicted CCSNe discovery rates for both the full galaxy catalogue (HSFG, LSFGs and additional bright galaxies) and for the lower-metallicity selections can be found in Table 2.5.

These predictions are a vast improvement on the rates predicted for the targeted survey strategy (Sections 2.3). Considering that the Pan-STARRS survey area is ~5.25 that of SDSS DR5, a total of ~570 CCSNe yr^{-1} are expected to be discovered (assuming that a complete galaxy catalogue for the survey volume can be compiled). Roughly 13 of these CCSNe are expected to be hosted by galaxies with $12+\log(O/H) < 8.2$. The number of CCSNe predicted to be discovered within the low-metallicity host galaxies can be considered as a lower-limit as the SDSS DR5 sample of blue, compact, dwarf galaxies within the proposed survey volume is probably not complete. The PS1 survey will provide a photometric catalogue of at least the quality the depth of SDSS DR5 (most likely significantly better) over 3π of the sky and hence provide a means to identify SNe in nearby, faint blue hosts. The number of low-metallicity CCSNe predicted to be discovered within a PS1 volume-limited survey is ~50% times more than predicted for the target survey strategy using a network of seven 2.0-m telescopes and ~1000 hrs of dedicated observing time. It thus seems much more efficient to use the PS1 survey to discover these objects than invest in a dedicated targeted survey strategy using large numbers of 2.0-m telescopes with standard CCD cameras and fields of view.

2.4.3 Predicted discovery rates for PS4. Eventually three more 1.8-m telescopes identical to PS1 will be added to the Pan-STARRS network to create PS4. These four telescopes will be trained on the same area of the sky simultaneously to effectively perform a deeper all-sky survey (with the same observing strategy as PS1), producing a co-added 25σ limiting magnitude of g=22.2 in a single epoch.

With an *apparent* limiting magnitude of $m_g = 21.5$, PS1 has an *absolute* limiting magnitude $M_g = -14.7$ at the boundary of the volume-limit survey ($z = 0.04$). To detect the same fraction of CCSNe as predicted for PS1, the boundary of a PS4 volume-limit survey can be pushed out to the point where the absolute limiting magnitude is identical to that of the PS1 survey, *i.e.* $z = 0.056$. Using the same volume-limited survey strategy as proposed for PS1 and introducing this new redshift limit, PS4 is predicted to discover a total of ~1,308 CCSNe yr^{-1}, ~ 18.3 of which are predicted to be hosted by galaxies with $12+\log(O/H) < 8.2$. These results can be found in Table 2.6.

	Total Sample		Detected CCSNe yr^{-1}	
12+log(O/H)	**Galaxies**	**CCSNe yr^{-1}**	**SDSS Area**	**PS1 Area**
No Limit	25,091	162.4	108.6	570.4
< 8.4	9,776	13.9	10.3	54.1
< 8.3	5,315	7.2	5.3	28.0
< 8.2	2,114	3.2	2.4	12.5
< 8.1	653	1.1	0.8	4.3

Table 2.5: Estimated intrinsic and discovered CCSRs within the SDSS DR5 survey area and $z < 0.04$. Also shown are the rates extended to the PS1 survey area.

	Total Sample		Detected CCSNe yr^{-1}	
12+log(O/H)	**Galaxies**	**CCSNe yr^{-1}**	**SDSS Area**	**PS4 Area**
No Limit	42,335	372.4	249.1	1,308.0
< 8.4	12,104	24.6	18.3	95.8
< 8.3	6,053	11.6	8.6	45.2
< 8.2	2,309	4.7	3.5	18.3
< 8.1	680	1.2	0.9	4.8

Table 2.6: Estimated intrinsic and discovered CCSRs within the SDSS DR5 survey area and $z < 0.056$. Also shown are the rates extended to the PS4 survey area.

2.5 Survey Strategy 3: A Magnitude-limited search with future all-sky surveys

Thus far when considering the Pan-STARRS all-sky survey to search for CCSNe the survey strategy has been volume-limited. If the aim is to discover *all* CCSNe possible of detection, then the Pan-STARRS survey is not being utilized to its greatest potential. A magnitude-limited survey with Pan-STARRS would be a more powerful strategy, as it would then be possible to discover SNe out to the distance limit imposed by the limiting-magnitude of the survey. This strategy is essentially the 'blind-survey' strategy followed by surveys such as the *Nearby SN Factory* (Copin et al. 2006). The inherent difficulty encountered with this strategy is trying to distinguish SNe from all other transient events and variables such as classical novae, asteroids and AGN and further distinguishing CCSNe from the thermonuclear (Type Ia) SNe. Assuming that it is possible to overcome these difficulties (and that transient events can be probabilistically classified) the number of CCSNe that a magnitude-limited survey strategy with PS1 and PS4 can be predicted and extrapolated to other future all-sky surveys like the Large Synoptic Survey Telescope (LSST) set to come online after 2016.

To determine the total CCSRs expected from the all-sky surveys PS1, PS4 and LSST, it must first be ascertained to what redshift-limit the SDSS DR5 galaxy sample

FILTER	PS1	PS4	LSST
g	21.5	22.2	22.7
r	20.9	21.7	22.4
i	20.8	21.6	21.8
z	19.8	20.6	21.2
Y	18.4	19.1	19.9

Table 2.7: The 25σ AB limiting magnitudes for PS1, PS4 and LSST

is complete to. When choosing spectroscopic targets SDSS DR5 has a lower magnitude limit of $r = 17.77$. This apparent magnitude-limit equates to an absolute magnitude limit of $M_r = -18$ at a redshift of $z = 0.033$. The galaxy density distribution for SDSS DR5 can be seen in Figure 2.10. There is a clear drop in the observed galaxy density at this redshift and so it is assumed that the SDSS DR5 galaxy sample is complete to this limit.

With this completeness limit in mind the local galaxy sample ($z < 0.033$) can be extrapolated out to the observable redshift limits of the all-sky surveys considered. It is assumed that the galaxy distribution throughout the observable universe is both homogeneous and isotropic. To determine the observable redshift limits of each all-sky survey it is necessary to model the CCSN detection distribution for each of the surveys. This is done by simulating a magnitude-limited survey to predict the percentage CCSNe detected as a function of redshift.

2.5.1 Survey simulation parameters. The simulation for the magnitude-limited survey strategy contain many of the same parameters as used for the targeted and volume-limited survey simulations (Sections 2.3.1 and 2.4.1).

The variant parameters that define one all-sky survey from another are the cadence and the limiting magnitudes of the surveys. The PS1 and PS4 magnitude-limited survey simulations incorporate the cadence defined for the Pan-STARRS observing strategy (Figure 2.8) and the 25σ limiting-magnitudes outlined by Chambers (2007), assuming that the limiting magnitude of PS4 is achieved via co-adding four PS1 images (see Table 2.7).

In the current proposed LSST configuration the telescope has an 8.4-m diameter with a 9.6 square degree field-of-view. It is planned that LSST will survey the whole of the observable sky every 3 nights, eventually covering a total of 20,000 square degrees. The primary focus of the survey is to detect transients. To detect fast, faint transient

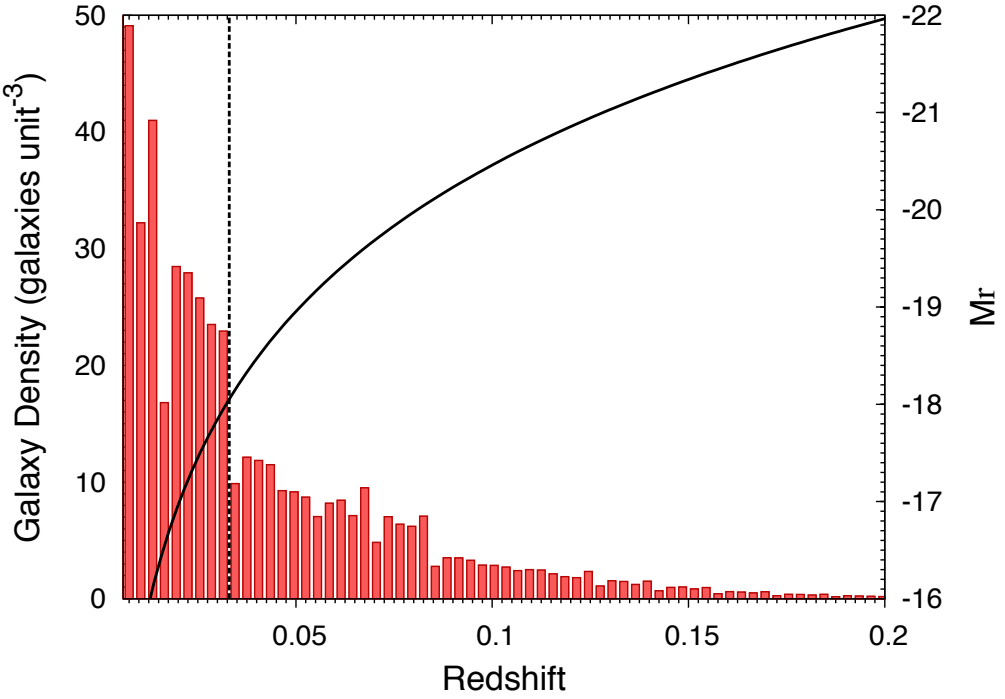

Figure 2.10: The galaxy distribution from the SDSS DR5 spectroscopic survey. The solid curve represents the *absolute* magnitude restiction of the SDSS spectroscopic target selection (apparent magnitude $r < 17.77$) as a function of redshift. An absolute magnitude-limit of $M_r = -18$ is reached at at redshift of 0.033 (dashed line). There is a clear drop in the galaxy density at this redshift and so this limit is chosen as the completeness limit of the SDSS DR5 galaxy sample.

events the sky will be surveyed with duplicate pairs of 15 sec exposures. Single exposure 25σ limiting-magnitudes calculated with the LSST exposure calculator are found in Table 2.7.

With a magnitude-limited survey strategy it is important to note that CCSNe shall be detected at relatively large redshifts compared to the volume-limited strategy. With this increase in survey depth, parameters that have previously been neglected, as the surveys have been relatively shallow, now have to be considered. These parameters include the star-formation history (SFH) of the universe, the redshifting of light emitted by the CCSNe, the broadening of the CCSNe lightcurves due to time-dilation and the retardation of the CCSN rates again due to time-dilation.

Star-formation history: As star-formation was more prolific earlier in the Universe's history than it is at present, star-formation is seen to increase with redshift (at least to moderate redshifts of $z \sim 2.5$). It is also important to note that approximately 50% of local star-formation activity is obscured, while at a redshift of z~1 this fraction could be as high as 80% (Takeuchi et al. 2005). To incorporate SFH into the magnitude-

limited survey simulations, also taking into account that a greater fraction of this star-formation will be obscured by dust at higher redshifts, the far-ultraviolet (FUV) SFR evolution determined by Schiminovich et al. (2005) is used (Equation 2.13).

$$\dot{\rho}_*(z) = (1+z)^{2.5\pm0.7} \tag{2.13}$$

Compared with all other indicators of SFR, the FUV luminosity is the most sensitive to dust. By using this indicator it is hoped that only star-formation that gives rise to CCSNe that are not too extinguished to be discovered in the survey considered.

***K*-Corrections:** Comparing the bolometric fluxes of objects at various redshifts presents no difficulty, as the total flux emitted by the objects at all wavelengths is being compared. However, in practice only a fraction of the total flux of an object is measured; redshifted and transmitted through a given bandpass. This presents a challenge as so far only the rest-frame (or emitted-frame) CCSN magnitudes have been considered but now their redshifted-frame (or observed-frame) magnitudes must be considered. To do this a transformation known as the *K*-correction (Oke and Sandage 1968; Hogg et al. 2002) must be determined to transform between emitted-frame and observed-frame magnitudes:

$$m_R = M_Q + \mathrm{DM} + K_{QR} \tag{2.14}$$

where m_R is the apparent magnitude of the object as measured through observed-frame bandpass, M_Q is the absolute magnitude of the object as measured through the emitted-frame bandpass, DM is the distance modulus of the object as determined from its luminosity distance and K_{QR} is the *K*-correction that transforms between these magnitudes. The *K*-correction can be understood as the difference in magnitude between two identical objects placed at the same distance; one traveling at a redshift z relative to the observer and measured through the observed-frame bandpass, the other at rest relative to the observer and measured through the emitted-frame bandpass (For more details on the *K*-correction see Appendix A).

The *K*-correction derived by Hogg et al. (2002) is used to account for the redshifting of the SN light in the survey simulation:

$$K_{QR} = -2.5\log_{10}\left[\frac{1}{[1+z]}\frac{\int \lambda_{obs}F_\lambda(\lambda_{obs})R(\lambda_{obs})\mathrm{d}\lambda_{obs}\int \lambda_{em}S^Q_\lambda(\lambda_{em})Q(\lambda_{em})\mathrm{d}\lambda_{em}}{\int \lambda_{obs}S^R_\lambda(\lambda_{obs})R(\lambda_{obs})\mathrm{d}\lambda_{obs}\int \lambda_{em}F_\lambda([1+z]\lambda_{em})Q(\lambda_{em})\mathrm{d}\lambda_{em}}\right] \tag{2.15}$$

where $F_\lambda(\lambda)$ is the spectral flux density of the object measured from spectral data (measured in ergs cm^{-2} s^{-1} Å^{-1}). $R(\lambda)$ and $Q(\lambda)$ are the observed-frame and emitted-frame

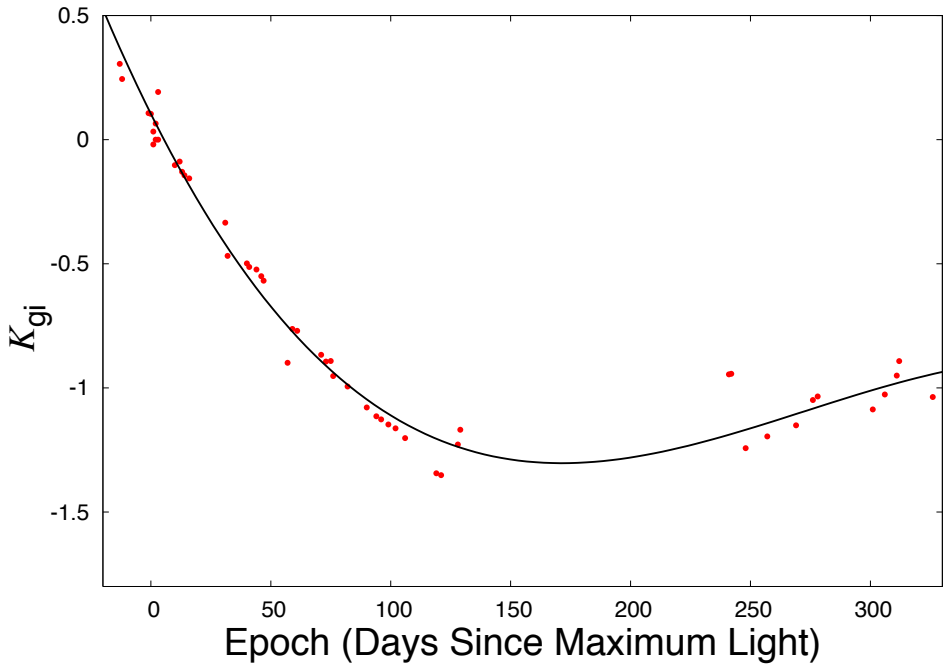

Figure 2.11: To cover the temporal range of CCSN evolution required by the magnitude-limited survey simulations, a third order polynomial is fitted to a set of K-correction data ($K_{gg}, K_{gr}, K_{gi}, K_{gz}$ or K_{gy}). The K-correction depends on the type, redshift and age of the CCSN observed. This example is of the K_{gi} correction for Type IIL SNe as sampled at a redshift of $z = 0.2$.

filter total throughput functions which depend on various parameters of the survey including the total throughput of the atmosphere, the reflectivity of the telescope mirrors, the transmission of the corrector optics and filters and the quantum efficiency of the camera detector. $S^R_\lambda(\lambda)$ and $S^Q_\lambda(\lambda)$ are the spectral flux densities for the AB zero-magnitude standard source as measured through the observed-frame and emitted-frame filters respectively. The AB zero-magnitude standard is a synthetic source equal to 3631 Jy (where 1 Jy = 10^{-26} W m^{-2} Hz^{-1}) at all frequencies (Oke and Gunn 1983).

It is necessary to K-correct each CCSN simulated to determine accurate apparent magnitudes as measured through each of the Pan-STARRS filters. The K-correction depends on four parameters; the filter used for observation, the type of CCSN observed, the redshift and age of the CCSN. Depending on which filter is used for observation, there are five possible K-corrections used in the simulation; $K_{gg}, K_{gr}, K_{gi}, K_{gz}$ or K_{gy}. As the K-correction is dependent on the type of CCSN observed, it is necessary to use appropriate archival spectral information to simulate the K-correction. SNe Type IIP the are represented by SN 1999em (spectra from Hamuy et al. 2001; Leonard et al.

2001; Baron et al. 2000), Type IIL by SN 1998S (spectra from Fassia et al. 2000; Pozzo et al. 2004; Fransson et al. 2005) and Type Ibc by SN2002ap (spectra from Gal-Yam et al. 2002) with spectral data supplemented by SN 1990B (Matheson et al. 2001, and the Asiago Catalogue) and SN 1998bw (Patat et al. 2001). As Type IIn/P and IIn/L are relatively rare, there is not enough spectral data to cover both the time and wavelength coverage required to simulate a full range of *K*-corrections. To compensate for this lack of data, the Type IIn/P population are represented by SNe Type IIP and the Type IIn/L population by SNe Type IIL. As each simulated CCSN is placed at a random distance/redshift, the representative CCSN spectral data must be redshifted to the given redshift and the observed-frame flux measured through the appropriate filter. Each simulated CCSN is also first observed at a random point in its evolution, therefore to accurately estimate the appropriate *K*-correction a third-order polynomial is fitted to a set of *K*-corrections defined by the CCSN type, observational filter and redshift to provide a *K*-correction for all stages of the CCSN evolution required by the simulation (See Figure 2.11)

It is imperative to have enough spectral information for each type of CCSN to cover the shear expanse of the parameters involved in estimating the *K*-corrections in the simulation. Spectral information is required to cover a large range of the evolution of each CCSN type including the rise to maximum light through to over 300 days post-explosion to accommodate for the maximum time separating two consecutive observations with the same filter according to the Pan-STARRS observation strategy (Figure 2.8). A wide range in wavelength coverage is also required of the spectral data to provide enough information to determine *K*-corrections for all five filters whenever possible, remembering that spectral data shall be redshifted according to the distance appointed to the CCSN by the simulation.

Time Dilation: The broadening of the CCSN lightcurves due to time dilation at relatively high redshift can be described simply as watching these CCSNe evolve in slow-motion with respect to our frame of reference. This enables a greater frequency of lightcurve sampling for the higher redshift CCSNe. The cadence hence goes as:

$$\text{cadence} = \text{cadence}_{\text{rest}} \times (1 + z). \tag{2.16}$$

The same argument leads to a retardation of the detected CCSN rates, giving:

$$\text{CCSR} = \text{CCSR}_{\text{rest}}/(1 + z). \tag{2.17}$$

2.5.2 Predicted discovery rates for PS1, PS4 and LSST. Figure 2.12 shows the CCSN detection distributions for PS1, PS2 and LSST. Beyond the redshift-limits set by

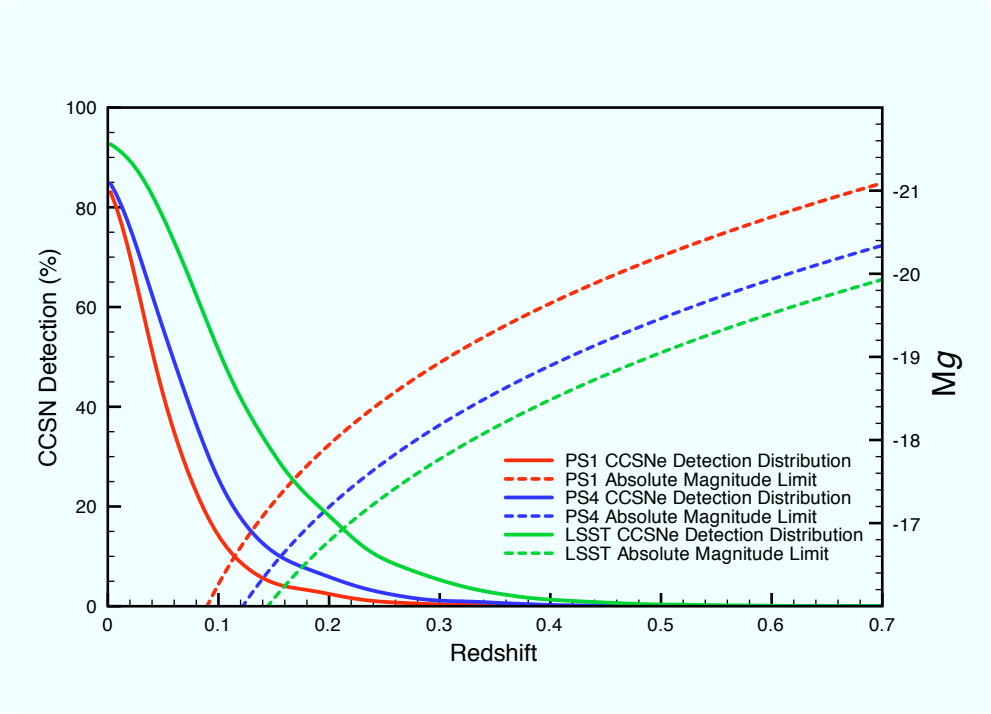

Figure 2.12: The solid lines show CCSN detection distributions for PS1, PS4 and LSST. The dashed lines are the absolute magnitude-limits of the surveys (a function of redshift). PS1, PS4 and LSST reach an absolute limiting magnitude of $M_g = -20$ at $z \sim 0.4$, $z \sim 0.5$ and $z \sim 0.6$ respectively.

an absolute limiting-magnitude of $Mg = -20$, the magnitude-limited surveys will cease to detect all but the most extreme luminosity CCSNe. It is at these redshift-limits that we choose to mark the boundary of the various magnitude-limited surveys; $z = 0.37$, $z = 0.50$ and $z = 0.59$ for PS1, PS4 and LSST respectively.

Assuming that galaxy density is homogeneous and isotropic throughout these survey volumes, the survey simulations extrapolates the nearby sample of galaxies ($z < 0.033$) with their predicted CCSRs to the sky coverages and redshift-limits of the three surveys. The simulation accounts for the SFH of the universe, the redshifting of light from distant CCSNe and theme-dilation of both the CCSN lightcurves and the CCSRs. Using the CCSN detection distributions obtained from the simulations (Figure 2.12) the CCSNe discovery rates of each survey are predicted. The results can be found in Table 2.8.

	Detected Core-Collapse SN Rates (SNe yr^{-1})			
12+log(O/H)	**DR5 Sample** ($z < 0.033$)	**PS1**	**PS4**	**LSST**
No Limit	103.5	24,095	68,620	160,249
< 8.4	9.8	3,046	8,343	19,627
< 8.3	5.3	1,640	4,491	10,566
< 8.2	2.3	786	2,153	5,064
< 8.1	0.9	278	762	1,794

Table 2.8: Predicted CCSRs for PS1, PS4 and LSST

2.6 Discussion and comparison with other surveys

Three different survey strategies designed to search for CCSNe, specifically in low-metallicity environments, a targeted survey of catalogued low-metallicity galaxies using a single or a network of 2.0-m telescopes, a volume-limited survey using the Pan-STARRS all-sky survey and a magnitude-limited survey using future all-sky surveys have been explored and their CCSN discovery rates simulated.

Using a single 2.0m telescope to perform a targeted survey of low-metallicity galaxies within $z = 0.04$ approximately 1.3 CCSNe yr^{-1} shall be discovered in host galaxies of with oxygen abundances $12 + \log(\mathrm{O/H}) < 8.2$. Using a network of seven 2.0-m telescopes to perform a targeted survey increases this number to ~9.3 CCSNe yr^{-1}. The relative number of similar events predicted to be discovered using a volume-limited survey with PS1 is estimated as ~12.5 CCSNe yr^{-1} and with PS4 as 18.3 CCSNeyr^{-1}. A drawback of the targeted low-metallicity survey is the ~1,000 hrs of telescope time would be required of a network of seven 2.0-m telescopes. Unlike the network of 2.0-m telescopes, all-sky surveys have the additional advantage of not being limited by the number of galaxies that they can feasibly observe and as a result shall be capable of observing CCSN events in all environments and not only those in the lowest-metallicity host galaxies, helping reduce the possibility of missing any rare CCSN events of extreme interest and also gaining the capability of determining accurate relative rates of SNe within a large but limited volume. A total of ~570 CCSNe yr^{-1} are expected to be discovered with PS1 and ~1,300 CCSNe yr^{-1} with PS4.

To estimate the amount of 8.0-m telescope time that would be required to spectroscopically follow the ~13 low-metallicity CCSNe found with the PS1 volume-limited survey, a typical CCSN discovered by the survey is considered. Depending on how early this SN is caught, the aim is to observe it at various epochs during its evolution and into its tail phase. Suggesting an average absolute magnitude of -15 for these epochs equates as an observed apparent magnitude of 20.7 at 120 Mpc (the mean discovery distance with $z < 0.04$), including a typical galactic extinction of 0.3 magnitudes.

To determine the time required from a typical 8.0-m telescope for spectroscopic follow-up we use the VLT FORS2 exposure time calculator, selecting a suitable grism (GRIS 300V), a 1″ slit and requiring a mean signal-to-noise of 20σ for each spectrum. To reach this signal-to-noise level we would require a ~700 sec on source integration. To spectroscopically follow the 13 events per year, requiring 5 epochs of observations per SN, would require ~13 hrs of 8.0-m telescope time per year.

An obstacle that would hinder both the targeted survey of low-metallicity galaxies and the volume-limited Pan-STARRS surveys is the incompleteness of any galaxy catalogue that can presently be produced. In the case of the wide area survey of Pan-STARRS one would ideally have a catalogue of all potential low-metallicity systems within the local Universe so that new discoveries could be quickly cross-matched and the optical transients in these galaxies immediately selected for follow-up. Hence it would be extremely useful to have an SDSS DR5 type catalogue covering the entire sky. As previously discussed (see 2.3.3) it is currently possible to compile a catalogue of $\sim 10^5$ galaxies within the sky area covered by Pan-STARRS and $z < 0.04$. This catalogue is far from complete, however when PS1 completes a full cycle of sky deep photometric catalogue of galaxies in the PS1 area can be compiled.

It will be challenging to identify and select genuine CCSNe in the magnitude-limited survey strategy. Without a defined volume-limit it becomes impossible to describe accurate relative rates of SNe and without the prior knowledge of the SN hosts it will be very difficult to segregate CCSNe from the large numbers of other transitory events, especially the more distant SNe Type Ia in apparently faint (but perhaps intrinsically bright) hosts. Most SNe are likely to be too distant to have any catalogued host and one of the challenges is to classify objects from the information gathered in the all-sky surveys themselves *e.g.* lightcurve matching, identification and photometric redshift measurement of the host, estimated energy of the transient. If it is possible to overcome these challenges the numbers of detected CCSNe expected from these unbiased, all-sky magnitude-limited surveys shall overwhelm those numbers from the other survey strategies by over an order of magnitude (see Tables 2.5, 2.6 and 2.8).

A pioneering survey using the magnitude-limited strategy has been the Texas Supernova Search (TSS), which has now evolved into the ROTSE Supernova Verification Project (RSVP) (Quimby et al. 2005; Yuan et al. 2007). The most remarkable result of this small scale SN survey is that they have claim over the discovery of the four of the most luminous SN ever detected; SN 2006tf (-20.7 mag), SN 2006gy (-22 mag), SN 2005ap (-22.7 mag) and SN 2008es (-22.5 mag). SN 2006tf and SN 2006gy were both classified as a Type IIn (Quimby et al. 2007; Quimby 2006) and possibly had Luminous Blue Variable (LBV) star progenitors (Smith 2008; Smith et al. 2007). SNe

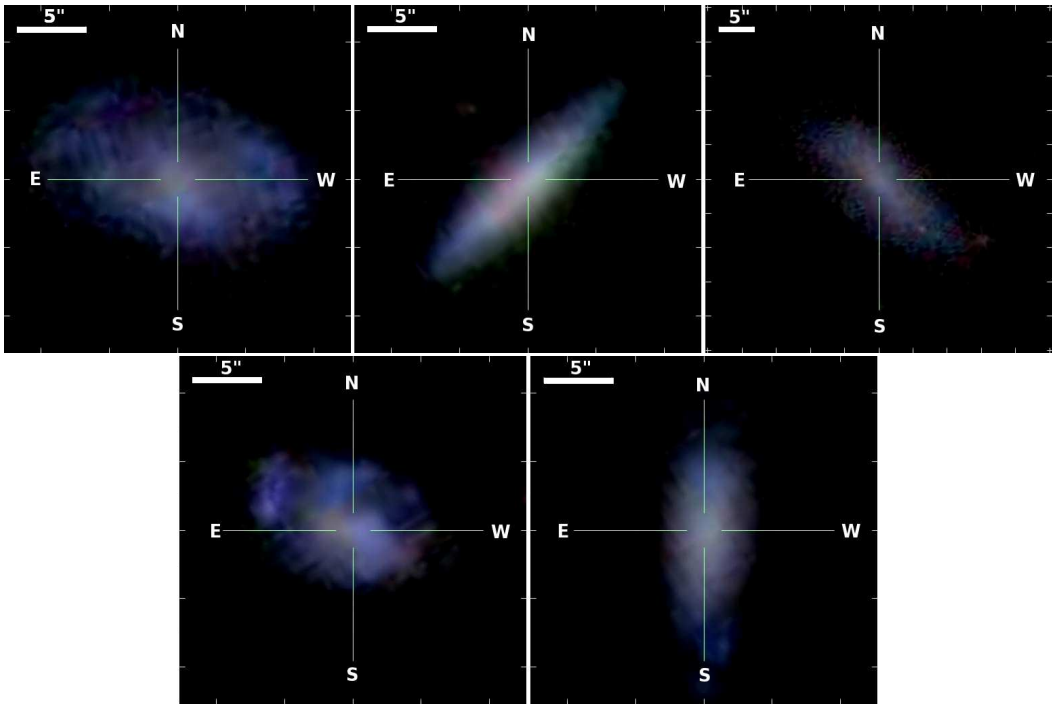

Figure 2.13: Of the 12 SNe discovered by the Nearby Supernova Factory that were hosted by SFGs in the SDSS DR5 catalogue, 5 were hosted by galaxies with 12+log(O/H) < 8.4. The host shown are SDSS J140737.23+384047 (SN 2007fg), SDSS J160205.11+294338 (SN 2007fz), SDSS J135042.68+400208 (SNF20080324-010), SDSS J154404.32+275335 (SNF20080515-004) and SDSS J150031.40+552210 (SNF20080614-002).

2005ap (Quimby et al. 2007) and 2008es (Gezari et al. 2009; Miller et al. 2009) were classified as a Type II and exhibited a broad Hα P-Cygni profile. The explosion of the progenitor of SN 2005ap, which still had its Hydrogen envelopes intact, has been speculated to have possibly been powered by a GRB type engine or a pair-instability eruption (Quimby et al. 2007). Although these type of super-luminous SNe may be intrinsically rare, it is more likely that they have remained undiscovered in the past due to the fact that they have been missed or misclassified as AGN in targeted surveys as they have occurred close to the cores of bright galaxies. The image-subtraction techniques used by area surveys, such as TSS and RSVP, will ensure that these types of interesting events will continue to be discovered. Taking a spectrum of the SN Type IIn 1998S at peak Fassia et al. (2000) to estimate the K-corrections that SNe similar to SN 2006gy would require, it is predicted that these events would be discovered out to $z \sim 0.6$ for PS1, $z \sim 0.8$ for PS4 and $z \sim 0.9$ for LSST. For PS4 and LSST these limits correspond to a search volume ~ 2.9 and ~ 4.4 times greater than PS1.

The Nearby Supernova Factory (NSF) uses ultra-wide field CCD mosaic images

Magnitude Range	PS1 Predictions	Classified by NSF
< 16	3.5 %	3.5 %
16 - 17	6.1 %	5.9 %
17 - 18	12.6 %	3.5 %
18 - 19	20.3 %	47.1 %
19 - 20	25.4 %	40.0 %
> 20	32.2 %	0.0 %

Table 2.9: Comparison between the relative magnitudes of CCSNe predicted with a volume-limited ($z < 0.04$) survey with PS1 and those discovered within the same volume by the Nearby Supernova Factory.

from the Near-Earth Asteroid Tracking (NEAT) and Palomar-Quest survey programs with the aim of finding low-redshift SNe Ia (Aldering et al. 2002). Within a volume-limited ($z < 0.04$) survey with PS1 the predicted relative-rates of SNe II, SNe Ibc and SNe IIn are 57.8%, 38.2% and 4.0% and at mean redshifts of 0.0318, 0.0316 and 0.0321 respectively. In its lifetime[7] the NSF has discovered and classified 85 CCSNe within $z < 0.04$ with relative-rates of SNe II, SNe Ibc and SNe IIn of 67.1%, 20.0% and 12.9% at mean redshifts of 0.0283, 0.0292 and 0.0284 respectively. The reason that the relative-rates of CCSNe types predicted from a PS1 volume-limited survey and those discovered by the NSF are somewhat discrepant may be due in part to the photometric screening of SN candidates that the NSF perform prior to spectroscopically classifying candidates. The NSF aim to find young SNe Ia that are nearby yet are within the Hubble-flow and therefore seem to classify SN candidates that are on the rise and that are close to the limiting-magnitude of their search (R $\sim$ 20 mags), as can be seen from the relative-magnitude distributions of classified SNe in Table 2.9. However it could be argued that because of the high-metallicity bias of many current and historic SN surveys, the relative-rates of nearby CCSNe compiled by Smartt et al. (2009) and used in the simulations are also biased toward higher metallicity. A high-metallicity bias in these relative-rates would be seen as an over-estimation of the true SN Ibc to SN II ratio as seen when compared to the relative-rates discovered by the NSF. Further evidence supporting this hypothesis results from cross-matching NSF discovered SNe with the catalogue of SDSS DR5 SFGs within $z < 0.04$. A total of 12 CCSNe are matched with SDSS galaxies, 5 of which occurring in galaxies with 12+log(O/H)<8.4 (see Fig. 2.13). This high fraction of CCSNe discovered in low-metallicity environments may again be due to selection criteria of the NSF (possibly looking for SNe occurring in apparently faint hosts) but remains encouraging when planning to search for low-metallicity CCSNe with future all-sky surveys.

[7]Up until September 2007

Another future all-sky survey that has potential for discovering SNe is Gaia, the European Space Agency's 'super-Hipparcos' satellite with the objective of creating the most precise three-dimensional map of the Galaxy (Perryman 2005). The satellite shall have many other additional capabilities including the ability to discover nearby SNe (within a few hundred Mpc). Predicted for launch in December 2011 it is a potential competitor of Pan-STARRS and LSST. Belokurov and Evans (2003) have performed a feasibility study similar to this study for Gaia, and have predicted that the satellite shall detect ~1,420 CCSNe yr^{-1} using a magnitude-limited survey strategy. Capable of detecting objects brighter than 20th magnitude, 1.5 magnitudes brighter than the g=21.5 limit for PS1, Gaia has the ability to survey a volume of only an eighth of the depth that PS1 shall survey. Belokurov and Evans (2003) employed a galaxy catalogue which more than likely neglected low-luminosity galaxies, which would result in the CCSN rate being under-predicted by up to a factor of ~2 fewer SNe. Hence if we scale the Belokurov and Evans prediction by ~16 the final numbers are comparable with the PS1 estimates. The scaled Belokurov and Evans prediction, ~22,720 CCSNe yr^{-1}, is now very close to the rate predicted for PS1, ~24,000 CCSNe yr^{-1} (see Table 2.8). However, note that these numbers are likely somewhat over optimistic due to the treatment of host galaxy extinction in the simulation.

2.7 Conclusions

Having determined oxygen abundances, star-formation rates and CCSN rates for all spectroscopically typed star-forming galaxies in the SDSS DR5 within $z = 0.04$, Monte-Carlo simulations were used to predict the fraction of these CCSNe that are expected to be discovered using different survey strategies. Using a single 2.0-m telescope (with a standard CCD camera) to perform a targeted survey of catalogued galaxies a discovery rate of ~1.3 CCSNe yr^{-1} is predicted within a volume that will allow detailed follow-up with 4.0-m and 8.0-m telescopes ($z = 0.04$). With a network of seven 2.0-m telescopes this estimate increases to ~9.3 CCSNe yr^{-1}, although this would require more than 1000 hrs of telescope time allocated to the network. A volume-limited search with the PS1 all-sky survey should discover ~ 12.5 CCSNe yr^{-1} in low metallicity galaxies. Over a period of a few years this would allow for detailed study of their properties. By extending these calculations it is possible to determine the total numbers of CCSNe that can potentially be found in magnitude-limited surveys with PS1 (24,000 yr^{-1}, within $z \lesssim 0.6$), PS4 (69,000 yr^{-1}, within $z \lesssim 0.8$) and LSST (160,000 yr^{-1}, within $z \lesssim 0.9$) surveys.

All considered, a final strategy chosen to searching for CCSNe in low-metallicity environments shall realistically involve elements of a volume-limited and a magnitude-

limited all-sky survey strategy. A volume-limited galaxy sample can be used to accurately determine relative SN rates and have some prior knowledge of the host galaxy characteristics. A magnitude-limit survey will not exclude the potential discovery of rare CCSN events that would have otherwise been missed had only a volume-limited survey strategy been considered.

With the huge number of CCSNe predicted to be discovered, these all-sky surveys are set to serve as a catalyst concerning our understanding of CCSNe; including their varying characteristics with metallicity, the relative rates of the various types of SNe and of extremely rare events similar to SN 2006jc, SN 2006gy, SN 2007bi and possibly events the nature of which have not yet been observed.